Acta Metallurgica Sinica (English Letters) (2022) 35:389–396
https://doi.org/10.1007/s40195-021-01279-1

Selective Laser Melting of Al-7Si-0.5 Mg-0.5Cu: Effect of Heat Treatment on Microstructure Evolution, Mechanical Properties and Wear Resistance

Pei Wang[1] · Sijie Yu[1] · Jaskarn Shergill[2] · Anil Chaubey[3] · Jürgen Eckert[4,5,8] · Konda Gokuldoss Prashanth[4,6,7] · Sergio Scudino[2]

Received: 21 March 2021 / Revised: 26 May 2021 / Accepted: 27 May 2021 / Published online: 15 July 2021

Abstract
Al-7Si-0.5 Mg-0.5Cu alloy specimens have been fabricated by selective laser melting (SLM). In this study, the effects of solution treatment, quenching, and artificial aging on the microstructural evolution, as well as mechanical and wear properties, have been investigated. The as-prepared samples show a heterogeneous cellular microstructure with two different cell sizes composed of α-Al and Si phases. After solution-treated and quenched (SQ) heat treatment, the cellular microstructure disappears, and coarse and lumpy Si phase precipitates and a rectangular Cu-rich phase were observed. Subsequent aging after solution-treated and quenched (SQA) heat treatment causes the formation of nanosized Cu-rich precipitates. The as-prepared SLMs sample has good mechanical properties and wear resistance (compressive yield strength: 215 ± 6 MPa and wear rate 2×10^{-13} m^3/m). The SQ samples with lumpy Si particles have the lowest strength of 167 ± 13 MPa and the highest wear rate of 6.18×10^{-13} m^3/m. The formation of nanosized Cu-rich precipitates in the SQA samples leads to the highest compressive yield strength of 233 ± 6 MPa and a good wear rate of 5.06×10^{-13} m^3/m.

Keywords Selective laser melting · Al-Si-Cu-Mg alloy · Heat treatment · Microstructure · Mechanical properties · Wear properties

1 Introduction

Selective laser melting (SLM) is one of the additive manufacturing technologies that work with the assistance of computer-aided designs (CAD), and it is widely used for the fabrication of metallic components [1]. SLM offers many advantages compared with conventional processes in terms of process flexibility, cost reduction, and energy-saving [2–4]. This has triggered the development of novel alloys that are specific for the SLM process to fabricate components with improved performance and functionalities. Due to the demand and widespread applications in the aerospace and automotive industries, Al-based alloys have become one of the most widely used classes of materials fabricated by SLM [5, 6]. With the rapid expansion of the market demand,

Available online at http://link.springer.com/journal/40195

✉ Konda Gokuldoss Prashanth
kgprashanth@gmail.com

1 Additive Manufacturing Institute, College of Mechatronics and Control Engineering, Shenzhen University, Shenzhen 518060, China

2 Institute for Complex Materials, IFW Dresden, Helmholtzstraße 20, 01069 Dresden, Germany

3 Institute of Minerals and Materials Technology (IMMT), Bhubaneshwar 751013, Orissa, India

4 Erich Schmid Institute of Materials Science, Austrian Academy of Sciences, Jahnstraße 12, 8700 Leoben, Austria

5 Department of Materials Science, Chair of Materials Physics, Montanuniversität Leoben, Jahnstraße 12, 8700 Leoben, Austria

6 Department of Mechanical and Industrial Engineering, Tallinn University of Technology, Ehitajete tee 5, 19086 Tallinn, Estonia

7 CBCMT, School of Mechanical Engineering, Vellore Institute of Technology, Vellore, Tamil Nadu 632 014, India

8 Adjunct With National University of Science and Technology «MISiS», Leninsky Prosp., 4, 119049 Moscow, Russia

more and more SLM aluminum parts are produced, resulting in a decrease in production costs [7, 8].

Research on the SLM-processed Al-based alloys has been mainly focused on the mechanical properties and the wear behavior of Al-Si series alloys. Ma et al. [9] successfully fabricated Al-20Si alloy specimens with a high yield strength (374 ± 4 MPa) and ultimate tensile strength (506 ± 5 MPa). These values are higher than the strength of the same alloy produced by conventional casting (105 and 162 MPa, respectively) and extruded (155 and 190 MPa, respectively) counterparts. Prashanth et al. [10] revealed that SLM processing of Al-12Si results in a fine cellular structure (1 ± 0.3 µm cell size) yielding three times higher strength values than the yield strength (260 MPa) of conventional cast samples. There are several reports dealing with SLM processing of Al-12Si alloys and related composites [11, 12]. Compared to conventional cast samples, SLM-processed Al-10Si-Mg can reach a fully dense microstructure with finer features and higher performance, with especially the tensile strength reaching up to 500 MPa and a significant improvement of the wear resistance [13–16]. Similarly, other Al-Si alloy systems like Al-35Si and Al-50Si have been explored and reported accordingly [17, 18]. Increasing the volume of Si increases the strength of the material, and at the same time, the material gets more brittle. Hence, it has been advised to have a minimum amount of Si to have an optimized combination of strength and ductility. In most cases, the Al-*x*Si samples reach an ultimate tensile strength between 360 and 420 MPa depending on the experimental conditions. Even though some of the Al-*x*Si samples show a brittle behavior, they are tough making them a good candidate in applications involving compressive stresses [19, 20]. Hence, more than tensile properties, the compressive properties are of most interest.

However, the mechanical properties and wear resistance of the current Al-Si and Al–Si–Mg series alloys are difficult to be tailored to meet the demands that Al-based alloys require under working conditions [10, 21–23]. The addition of Cu and Mg elements into Al alloys is helpful to tailor the microstructure and the performance by different heat treatment procedures because of the precipitation of strengthening phases (e.g., θ, θ', and Mg_2Si). Wang et al. designed and fabricated an SLM Al-3.5Cu-1.5 Mg-1Si alloy, which shows improved mechanical properties and corrosion resistance [24–26]. In this work, a novel Al-7Si-0.5Cu-0.5 Mg alloy was designed and fabricated using the SLM process. Systematical investigations concerning the influence of solution treatment, quenching and artificial aging on the microstructure and mechanical properties of the SLM-processed Al-7Si-0.5Cu-0.5 Mg alloy parts have been performed, revealing that the as-prepared SLM sample shows the highest hardness and the hardness drops with solution treatment. Again, the hardness may be improved by artificial aging, but the hardness does not reach the values of the as-prepared samples.

2 Experimental

2.1 Materials and SLM Processing

Bulk specimens were produced by SLM from spherical gas-atomized powder (from TLS technique) with a nominal composition of Al-7Si-0.5Cu-0.5 Mg (wt%). Cylindrical rods for compression tests (Ø 3 mm × 6 mm height) and for wear tests (Ø 9 mm × 12 mm height) were fabricated using an SLM 250HL system (SLM Solutions Group AG) equipped with a 400 W Nd:YAG laser (continuous wave). The parameters used for preparing the samples were as follows: scanning speed of 1455 mm/s for the volume, power of 320 W for both volume and contour, layer thickness of 50 µm, hatch spacing of 110 µm, and straight-line hatch style with 73° rotation between the layers were employed, which is similar to most of the other Al-based alloys [27, 28]. The SLM processing was carried out under a protective argon atmosphere (Ar purity > 99%). The as-prepared SLM samples were thermally treated under the following two conditions: (1) 540 °C for 8 h—solution-quenched condition (SQ) and (2) 540 °C for 8 h + 190 °C for 20 h—age-hardened condition (SQA) under vacuum conditions in a vacuum furnace. The heating rate was maintained at 10 °C/min.

2.2 Characterization

Optical microscopy was carried out by using a VHX-2000 digital microscope (OM; Keyence). Phase analysis was performed by X-ray diffraction (XRD) using a D3290 PANalytical X'pert PRO diffractometer with Co-$K\alpha$ radiation ($\lambda = 0.17889$ nm) in Bragg–Brentano configuration. XRD phase analysis was performed on the cross section of the Al-7Si-0.5 Mg-0.5Cu alloys for two different heat treatment conditions. The microstructure of the samples was investigated by a scanning electron microscope (SEM; Gemini LEO 1530) equipped with an energy-dispersive X-ray spectroscopy system (EDS; Quantax 400 with SDD-Detector Xflash 4010, Bruker). The density of the samples was measured with the Archimedes method. The number and average width of particles were calculated from the OM/SEM images by using Image-Pro Plus software (Version 6.0 Software, Media Cybernetics, Inc. USA).

2.3 Mechanical Properties

Vickers microhardness tests were performed using an HMV Shimadzu microhardness tester with 0.01 kg load and 10 s dwell time. The hardness of each specimen is the

value averaged over at least 20 different points, which were selected automatically. Room-temperature compression tests were carried out with the loading axis parallel to the building direction (BD) using an Instron 5869 machine at a constant crosshead speed of 0.001 mm/s according to DIN 50,106 standard. A laser extensometer (Fiedler Optoelektronik GmbH, Germany) was used to measure the strain directly on the samples. At least five specimens were tested in the same condition to ensure the reproducibility of the results.

2.4 Sliding Wear Tests

Sliding wear tests were carried out according to the ASTM G 99–05 standard at room temperature and in ambient atmospheric conditions using a pin-on-disc test device. A disk of 45-mm diameter and 13-mm thickness made of hard-faced stainless steel was used against Al-12Si flat head pins of 9-mm diameter and 12-mm height. The tests were performed at constant load (10 N) with a sliding speed of 1 m/s for 30 min. The wear rate and the volume loss were calculated using Archard's equation, which can be found elsewhere [29].

3 Results and Discussion

3.1 Phase Evolution

Figure 1 shows the XRD patterns of the as-prepared SLM Al-7Si-0.5 Mg-0.5Cu samples along with the results for two different heat-treated conditions. The diffraction peaks of α-Al and Si are observed in the as-prepared SLM sample.

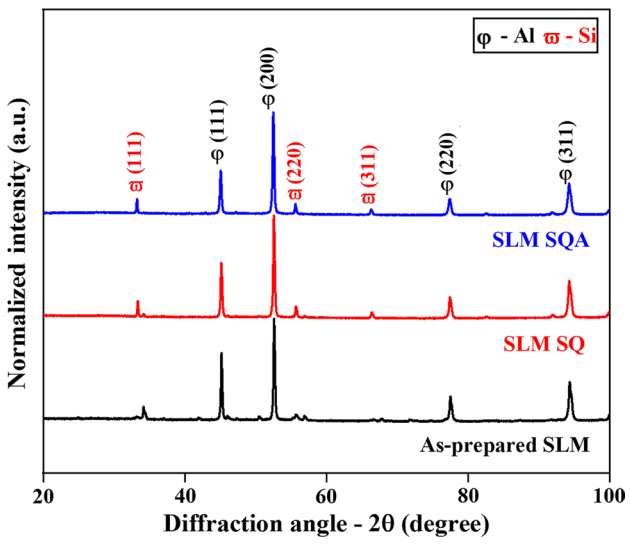

Fig. 1 X-ray diffraction patterns of the SLM Al-7Si-0.5 Mg-0.5Cu samples in as-prepared, solution-quenched (SQ) and solution-quenched, and artificially aged (SQA) conditions

Some small peaks related to the Mg_2Si precipitates are also observed in the as-prepared sample. The thermal treatment (SQ and SQA conditions) does not show the formation of a new phase(s), but the peak intensities of the existing phases change. The intensity of the Si peaks increases with thermal treatment, suggesting that the Si present in the supersaturated solution diffuses out of the Al matrix, as already observed in SLM Al-12Si specimens [10]. Irrespective of the changes in the peak intensities, the Al phase exhibits a crystallographic texture, similar to most of the SLM-processed alloys. The small peaks observed should correspond to Mg_2Si phase, which also disappears after solution treatment.

The lattice parameter of α-Al in the as-prepared condition is 0.405092 ± 0.000004 nm, and it changes to 0.405112 ± 0.000002 nm in the SLM SQ condition. This indicates that less Si is dissolved in the Al lattice as supersaturated solid solution after solution treatment and more free residual Si is observed (~3.5 wt%). With further aging, the lattice parameter increases to 0.405188 ± 0.000004 nm, clearly indicating additional diffusion of Si out of the Al lattice. This agrees well with the growth of the Si peaks in the SLM-SQA condition.

3.2 Microstructural Characterization

Figure 2 shows the microstructure of the SLM Al-7Si-0.5 Mg-0.5Cu samples in as-prepared and heat-treated conditions. As shown in Fig. 2a, there are no solidification defects in the as-prepared SLM samples except for the presence of anisotropy in the microstructure. The samples show a density of ~99.4%. The as-prepared SLM samples show a heterogeneous microstructure composed of both coarse and fine microstructural zones (Fig. 2a), which result from different thermal histories in the melt pool and the layer-by-layer processing strategies [29–32]. The coarse microstructure zone results from recrystallization of the microstructure caused by the heat-affected mechanism of the previous scanned track [30, 33] and has an average width of around 10–20 µm.

After heat treatment, the heterogeneous microstructure of the as-prepared SLM alloy disappears, and the SQ and SQA samples show a relatively homogeneous microstructure with an average number of particles of ~490 (observed from the OM images) and an average particle width of ~1.35 µm. The OM images of the SQA samples (Fig. 2c) contain more particles than in the SQ samples, and there are fewer rectangular particles. The average particle width in the SQA condition is found to be as similar as for the SQ samples, which is slightly larger than for SLM Al-Si10-Mg subjected to the same heat treatment protocol, which was fabricated and investigated by Li et al. [21].

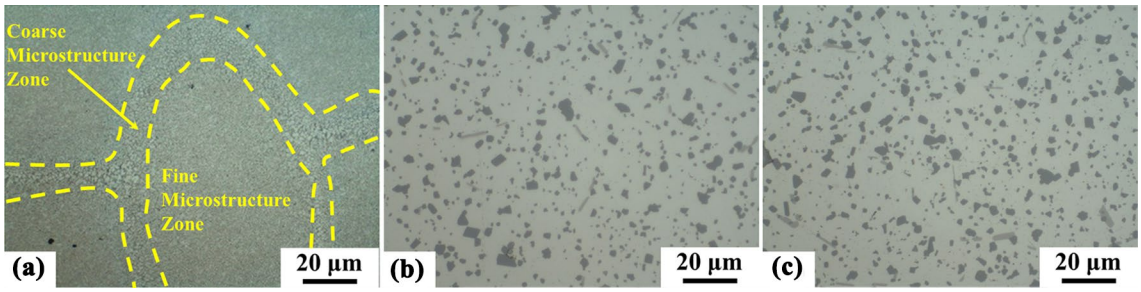

Fig. 2 Optical microscopy images of SLM Al-7Si-0.5 Mg-0.5Cu samples in (**a**) as-prepared, (**b**) solution-quenched, (**c**) solution-quenched artificially aged conditions

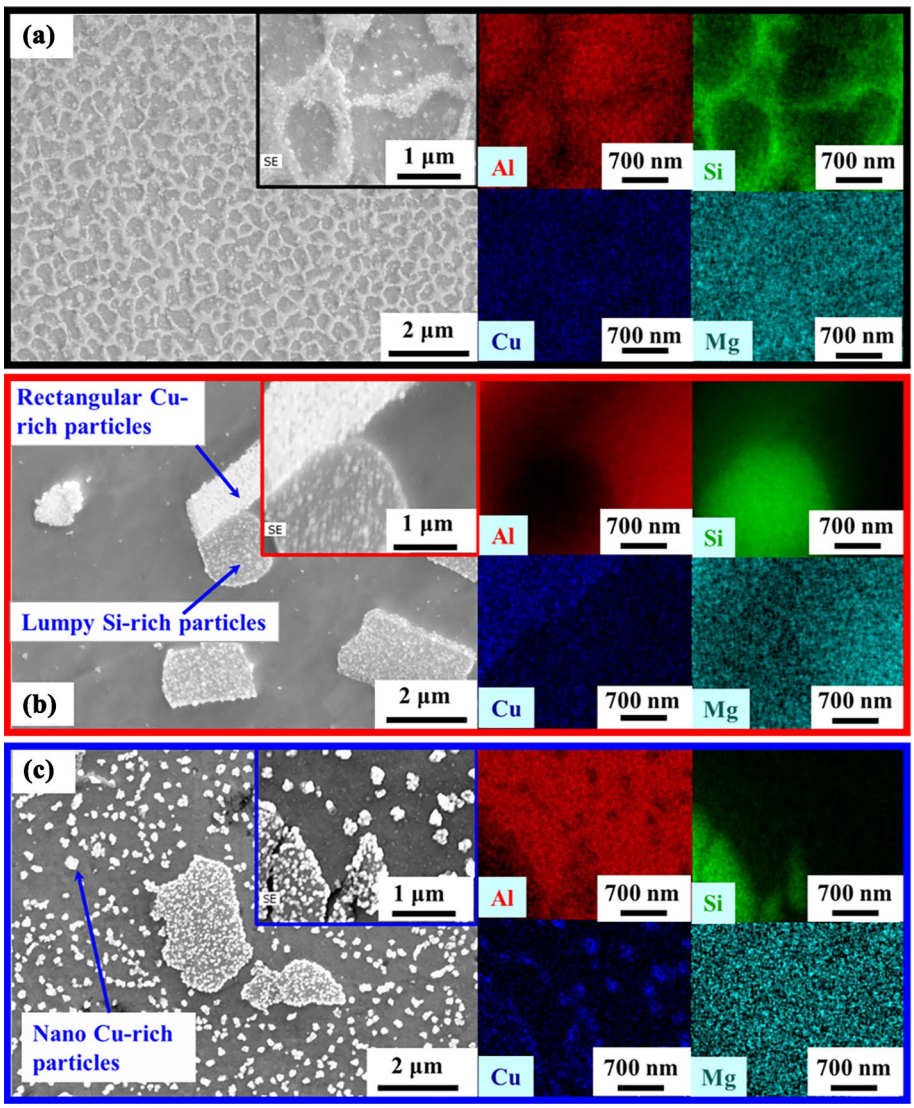

Fig. 3 Bright-field scanning electron microscopy images and corresponding energy-dispersive spectroscopy maps at high magnification for etched SLM Al-7Si-0.5 Mg-0.5Cu samples: (**a**) as-prepared, (**b**) solution quenching, (**c**) solution-quenched artificial aging

The microstructures of the SLM samples before and after heat treatment were observed by SEM and EDS and are shown in Fig. 3. The microstructure of the as-prepared samples consists of a fine equiaxed cellular α-Al matrix decorated with a eutectic fibrous Si network. Such a microstructural arrangement can be ascribed to the high cooling rate characterizing the SLM process [34–36]. The cellular microstructure disappears after SQ and SQA thermal treatments (Fig. 3b and c). According to EDS analysis, lumpy Si phases and rectangular-shaped Cu-rich phases form in the SQ samples (Fig. 3b), which precipitate from the excessive amount of solute in the supersaturated solid solution of Al. In addition, there is no Mg-rich zone in the SQ samples, indicating the complete dissolution of magnesium in the Al phase. As shown in Fig. 3c, granular nanosized Cu-rich phases precipitate after artificial aging of the SQ samples. Similar microstructures and precipitation behavior have been observed for Al-12Si alloy in the as-prepared and heat-treated conditions [10].

3.3 Mechanical Properties

The compressive yield strength, Vickers hardness, and wear rate of all the differently treated materials are shown in Fig. 4. The as-prepared samples show compressive yield strength of 215 ± 6 MPa because of the Orowan looping mechanism induced by the fibrous Si precipitate network [16]. The size effect plays a major role in strengthening of these materials. The loops induce elastic loading of the Si phases and produce back stresses in the Al matrix [37]. The internal stress of the matrix leads to kinematic hardening and a Bauschinger effect in precipitate-strengthened alloys [38]. It has been observed that the as-prepared SLM samples show a high degree of dislocation density (2–3 orders of magnitude more than their cast counterpart) [39, 40]. The fine microstructural features including grain boundaries block the dislocations, where they pile up. In addition, other dislocations also block the dislocation movement leading to the dislocation tangle. Moreover, based on Orowan's theory, the looping-induced internal stress increases with the decrease in interparticle spacing, leading to high strength in the as-prepared SLM samples. After SQ heat treatment, the cellular structure in the SLM-fabricated samples disappears, and the nanosized Si phase transforms into lumpy Si phase precipitates, which synergistically weakens the Orowan strengthening and leads to a decrease in the compressive yield strength after the solution treatment (167 ± 13 MPa) [10]. The dislocation density also decreases due to the influence of the thermal treatment. However, nanosized Cu-rich precipitates that form after further artificial aging significantly enhance strengthening through the Orowan mechanism, thereby leading to the highest compressive yield strength (in SQA samples) of 231 ± 6 MPa observed for all three sample conditions.

Hardness is also an important indicator of the material's capability to resist plastic deformation [41]. The as-prepared SLM Al-7Si-0.5Cu-0.5 Mg samples have a maximum microhardness of 190 ± 8 $HV_{0.01}$ because of the formation of a supersaturated solid solution caused by the high cooling rate realized upon SLM [9]. With the SQ heat treatment, the lumpy Si-rich phase and the rectangular Cu phase precipitate and the solid solution strengthening decrease, which leads to a lower hardness of the Al matrix than for the as-prepared SLM specimens. Therefore, the SQ samples exhibit the

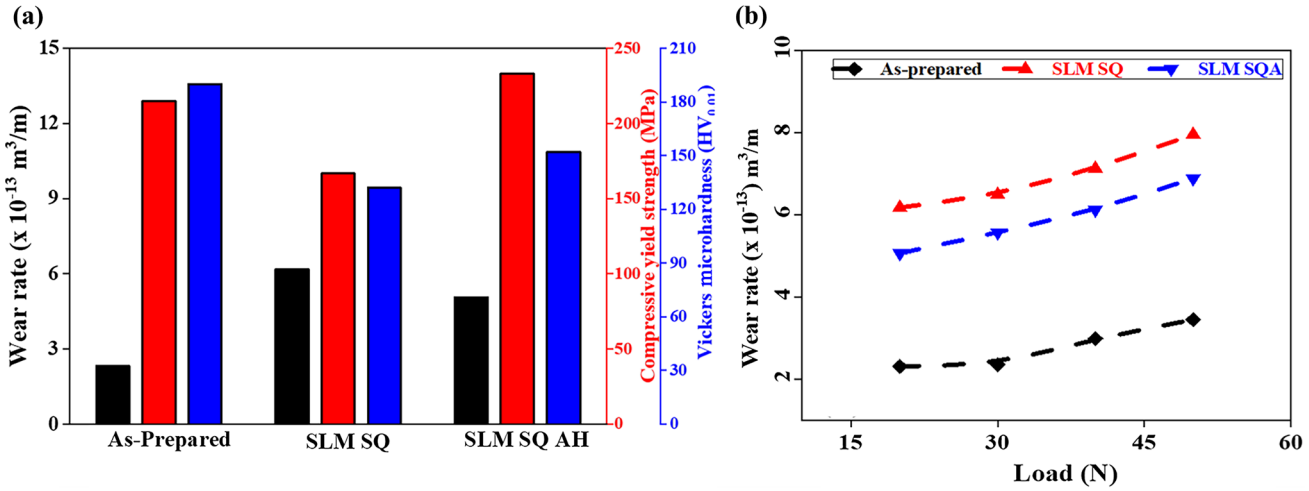

Fig. 4 (**a**) Wear rate (20 N load), compressive yield strength, and Vickers microhardness of SLM Al-7Si-0.5 Mg-0.5Cu samples in three different conditions (as-prepared, SQ, and SQA). Black bars represent the wear rate, red bars represent the compressive yield strength, and the blue bars represent the Vickers microhardness data. (**b**) Wear rate plotted as a function of load for the SLM-processed material in as-prepared and heat-treated conditions

lowest hardness of $132 \pm 12 HV_{0.01}$. The artificial aging leads to a uniform distribution of nanosized Cu particles, which strengthen the Al matrix and improve the hardness of the SQA specimens. Therefore, the SQA samples show a moderate hardness of 152 ± 5 $HV_{0.01}$, which is lower than that of the as-prepared samples but higher than that of the SQ samples. Generally, the hardness shows an inverse correlation with the wear rate [37], and the results show the same trend in Fig. 4(a). The as-prepared SLM Al-7Si-0.5 Mg-0.5Cu samples show the lowest wear rate of 2×10^{-13} m^3/m. The SQ samples exhibit a maximum wear rate of 6.18×10^{-13} m^3/m and after aging of the SQ samples, the wear resistance of the SQA samples improves again where the wear rate is reduced to 5.06×10^{-13} m^3/m.

Figure 5 depicts the morphology of the worn surfaces for the different types of materials. As shown in Fig. 5a1 and a2, the worn surfaces display groove tracks and contain little dropped debris as well as oxide particles and delamination, indicating abrasive wear features. The features are attributed to the presence of oxide particles, which are generally harder than the matrix. They may thus improve the wear resistance of the samples [42].

The delamination is mainly attributed to the orientation of tracks with respect to the surface in contact with the sliding disk [43]. The solution and quench post-heat treatment causes precipitation of the lumpy Si phase and decreases microhardness and compression strength. The reduction in the microhardness leads to furrows and cracks, and some fracture features are observed on the worn surface (Fig. 5b1 and b2). The SQ samples show significant adhesive phenomena, owing to the precipitation of lumpy Si particles [44]. As shown in Fig. 5c1 and c2, there is more debris in the image of the SQA samples due to the grinding of nanosized Cu particles during the wear test. Meanwhile, the nanosized Cu phase enhances the hardness of the material, which also leads to the formation of groove tracks upon loading. Therefore, the wear resistance of the SQA samples is affected by both adhesive and abrasive wear mechanisms.

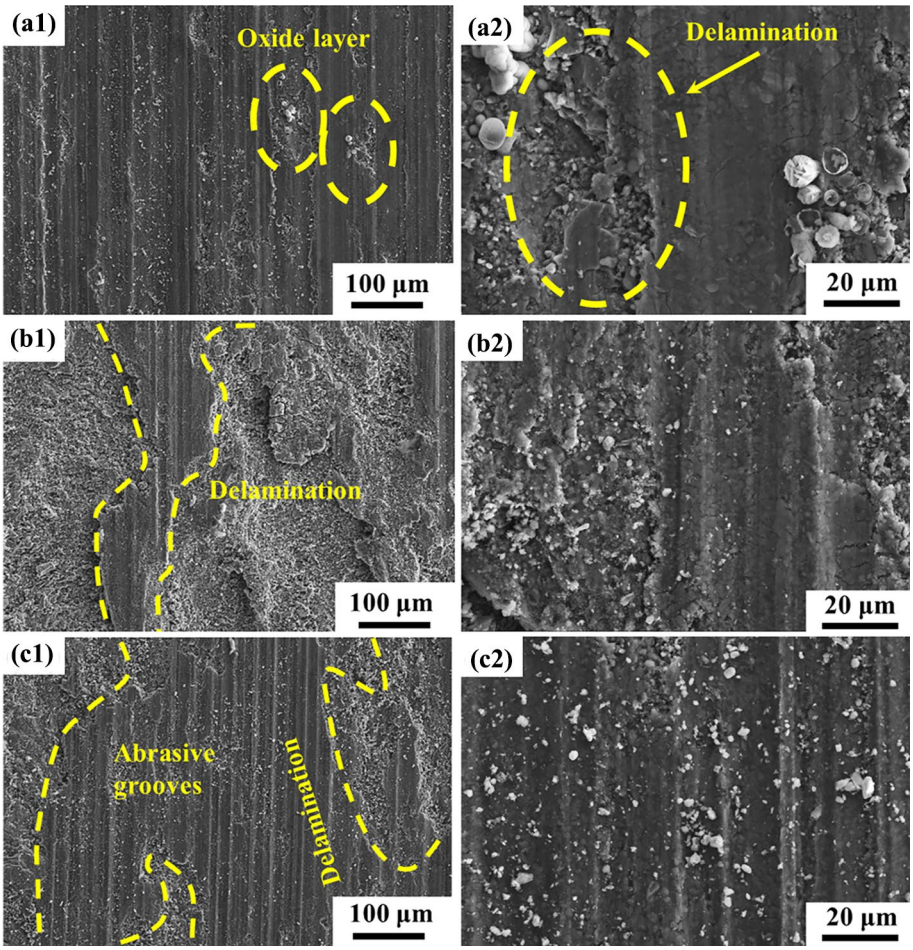

Fig. 5 Bright-field scanning electron microscopy images of the worn surfaces of (**a**) as-prepared, (**b**) solution-quenched, (**c**) solution-quenched artificially aged samples under low and high magnification after wear testing

4 Conclusions

In this study, fully dense Al-7Si-0.5 Mg-0.5Cu samples were successfully fabricated by SLM. The as-prepared SLM samples consist of a fine equiaxed cellular α-Al matrix decorated with a eutectic fibrous Si network. SQ heat treatment generates coarse and lumpy Si-rich and rectangular Cu-rich phases. Artificial aging leads to uniform precipitation of nanosized Cu-rich phases in the α-Al and Si phases.

The as-prepared SLM samples exhibit compressive yield strength of 215 ± 6 MPa and Vickers microhardness of 190 ± 8 $HV_{0.01}$. After SQ heat treatment, the compressive yield strength decreases to 169 ± 13 MPa, and the Vickers microhardness drops to 132 ± 12 $HV_{0.01}$. The SQA samples show the highest compressive yield strength of 231 ± 6 MPa and a reasonable Vickers hardness of 152 ± 5 $HV_{0.01}$. In addition, the as-prepared SLM samples have the lowest wear rate of 2×10^{-13} m^3/m and display abrasive wear features. In contrast, the SQ samples with the highest wear rate of 6.18×10^{-13} m^3/m show an adhesive worn surface. Due to mixed mechanisms of adhesive and abrasive wear, the SQA samples exhibit a good wear resistance and a moderate wear rate of 5.06×10^{-13} m^3/m.

Acknowledgements This work was financially supported by the Guangdong Basic and Applied Basic Research Foundation (2020A1515110869), Shenzhen International Cooperation Research (GJHZ20190822095418365) and the Natural Science Foundation of SZU (Grant No. 2019040). Additional support was provided by the European Regional Development Fund (ASTRA6-6). Jürgen Eckert is grateful for the support from the Ministry of Science and Higher Education of the Russian Federation in the framework of the Increase Competitiveness Program of MISiS (Support project for young research engineers, Project No. K2-2020-046).

References

[1] H. Attar, K.G. Prashanth, A.K. Chaubey, M. Calin, L.C. Zhang, S. Scudino, J. Eckert, Mater. Lett. **142**, 38 (2015)
[2] P. Didier, G. Le Coz, G. Robin, P. Lohmuller, B. Piotrowski, A. Moufki, P. Laheurte, J. Manuf. Proc. **62**, 213 (2021)
[3] H. Wu, Y. Dong, X. Li, Y. Li, M. Yan, Mater. Sci. Eng. A **803**, 140711 (2021)
[4] Y. Zhu, J. Zou, X. Chen, H. Yang, Wear **350**, 46 (2016)
[5] K. Bartkowiak, S. Ullrich, T. Frick, M. Schmidt, Phys. Proc. **12**, 393 (2011)
[6] J.P. Kruth, G. Levy, F. Klocke, T.H.C. Childs, CIRP Ann. Manuf. Technol. **56**, 730 (2007)
[7] M.K. Thompson, G. Moroni, T. Vaneker, G. Fadel, R. Ian Campbell, I. Gibson, A. Bernard, J. Schulz, P. Graf, B. Ahuja, F. Martinac, CIRP Ann. Manuf. Technol. **65**, 737 (2016)
[8] R. Liu, Z. Wang, T. Sparks, F. Liou, J. Newkirk, in *Laser Additive Manufacturing*. ed. by M. Brandt (Woodhead Publishing, Cambridge, 2017), p. 351
[9] P. Ma, K.G. Prashanth, S. Scudino, Y. Jia, H. Wang, C. Zou, Z. Wei, J. Eckert, Metals **4**, 28 (2014)
[10] K.G. Prashanth, S. Scudino, H.J. Klauss, K.B. Surreddi, L. Löber, Z. Wang, A.K. Chaubey, U. Kühn, J. Eckert, Mater. Sci. Eng. A **590**, 153 (2014)
[11] Z. Wang, R. Ummethala, N. Singh, S. Tang, C. Suryanarayana, J. Eckert, K.G. Prashanth, Materials **13**, 4564 (2020)
[12] P. Wang, J. Eckert, K.G. Prashanth, M. Wu, I. Kaban, L. Xi, S. Scudino, Trans. Nonferrous Met. Soc. China **30**, 2001 (2020)
[13] W.Q. Zhang, H.L. Zhu, Z.H. Hu, X.Y. Zeng, Acta Metall. Sin. **53**, 918 (2017)
[14] C. Gao, Z. Liu, Z. Xiao, W. Zhang, K. Wong, A.H. Akbarzadehq, J. Alloys Compd. **853**, 156722 (2021)
[15] D.H. Dai, D.D. Gu, M.J. Xia, C.L. Chen, H.Y. Chen, T. Zhao, C. Hong, A. Gasser, R. Poprawe, Surf. Coat. Technol. **349**, 279 (2018)
[16] B. Chen, S.K. Moon, X. Yao, G. Bi, J. Shen, J. Umeda, K. Kondoh, Scr. Mater. **141**, 45 (2017)
[17] Y.D. Jia, P. Ma, K.G. Prashanth, G. Wang, J. Yi, S. Scudino, F.Y. Cao, J.F. Sun, J. Eckert, J. Alloys Compd. **699**, 548 (2017)
[18] Y.D. Jia, L.B. Zhang, P. Ma, S. Scudino, G. Wang, J. Yi, J. Eckert, K.G. Prashanth, Prog. Addit. Manuf. **5**, 247 (2020)
[19] J. Suryawanshi, K.G. Prashanth, S. Scudino, J. Eckert, O. Prakash, U. Ramamurty, Acta Mater. **115**, 285 (2016)
[20] K.G. Prashanth, Mater. Des. Process. Commun. **1**, e46 (2019)
[21] W. Li, S. Li, J. Liu, A. Zhang, Y. Zhou, Q. Wei, C. Yan, Y. Shi, Mater. Sci. Eng. A **663**, 116 (2016)
[22] T. Kimura, T. Nakamoto, M. Mizuno, H. Araki, Mater. Sci. Eng. A **682**, 593 (2017)
[23] J.H. Rao, Y. Zhang, K. Zhang, A. Huang, C.H.J. Davies, X. Wu, Scr. Mater. **160**, 66 (2019)
[24] P. Wang, C. Gammer, F. Brenne, K.G. Prashanth, R.G. Mendes, M.H. Rümmeli, T. Gemming, J. Eckert, Mater. Sci. Eng. A **711**, 562 (2018)
[25] P. Wang, A. Gebert, L. Yan, H. Li, C. Lao, Z. Chen, K. Kosiba, U. Kühn, S. Scudino, Intermetallics **124**, 106871 (2020)
[26] P. Wang, C. Gammer, F. Brenne, T. Niendorf, J. Eckert, S. Scudino, Comp. Part B Eng. **147**, 162 (2018)
[27] P. Ma, Y. Jia, K.G. Prashanth, S. Scudino, Z. Yu, J. Eckert, J. Alloys Compd. **657**, 430 (2016)
[28] K.G. Prashanth, H. Shakur Shahabi, H. Attar, V.C. Srivastava, N. Ellendt, V. Uhlenwinkel, J. Eckert, S. Scudino, Addit. Manuf. **6**, 1 (2015)
[29] H.J. Rathod, T. Nagaraju, K.G. Prashanth, U. Ramamurty, Trib. Int. **137**, 94 (2019)
[30] X. Su, Y. Yang, J. Mater. Process. Technol. **212**, 2074 (2012)
[31] L. Thijs, K. Kempen, J.P. Kruth, J. Van Humbeeck, Acta Mater. **61**, 1809 (2013)
[32] Z. Wang, S.Y. Tang, S. Scudino, Yu.P. Ivanov, R.T. Qu, D. Wang, C. Yang, W.W. Zhang, A.L. Greer, J. Eckert, K.G. Prashanth, Addit. Manuf. **37**, 101725 (2021)
[33] K.G. Prashanth, J. Eckert, J. Alloys Compd. **707**, 27 (2017)
[34] P. Wang, L. Deng, K.G. Prashanth, S. Pauly, J. Eckert, S. Scudino, J. Alloys Compd. **735**, 2263 (2018)
[35] H.Y. Jung, S.J. Choi, K.G. Prashanth, M. Stoica, S. Scudino, S. Yi, U. Kühn, D.H. Kim, K.B. Kim, J. Eckert, Mater. Des. **86**, 703 (2015)
[36] Z. Wang, M. Xie, Y. Li, W. Zhang, C. Yang, L. Kollo, J. Eckert, K.G. Prashanth, NPG Asia Mater. **12**, 30 (2020)
[37] Z. Zhang, D. Chen, Scr. Mater. **54**, 1321 (2006)
[38] J. da Costa Teixeira, L. Bourgeois, C.W. Sinclair, C.R. Hutchinson, Acta Mater. **57**, 6075 (2009)
[39] C. Zhao, Z. Wang, D. Li, L. Kollo, Z. Luo, W. Zhang, K.G. Prashanth, Int. J. Plast. **138**, 102926 (2021)
[40] R. Ummethala, P.S. Karamched, S. Rathinavelu, N. Singh, A. Aggarwal, K. Sun, E. Ivanov, L. Kollo, I. Okulov, J. Eckert, K.G. Prashanth, Materialia **14**, 100941 (2020)

[41] D. Buchbinder, H. Schleifenbaum, S. Heidrich, W. Meiners, J. Bültmann, Phys. Proc, **12**, 271 (2011)
[42] B.R. Marple, R.S. Lima, J. Therm. Spray. Technol. **14**, 67 (2005)
[43] D.K. Dwivedi, Mater. Des. **31**, 2517 (2010)
[44] K.G. Prashanth, B. Debalina, Z. Wang, P.F. Gostin, A. Gebert, M. Calin, U. Kühn, M. Kamaraj, S. Scudino, J. Eckert, J. Mater. Res. **29**, 2044 (2014)